Available online at www.sciencedirect.com
SCIENCE DIRECT®
Journal of Solid State Chemistry 172 (2003) 178–187
JOURNAL OF SOLID STATE CHEMISTRY
http://elsevier.com/locate/jssc

A new octahedral tilt system in the perovskite phase $Ca_3Nb_2O_8$

L.M.D. Cranswick,[a] W.G. Mumme,[b] I.E. Grey,[b,*] R.S. Roth,[c] and P. Bordet[d]

[a] *CCCP14, Birkbeck University of London, London WC1E 7HX, UK*
[b] *CSIRO Minerals, Box 312 Clayton South, Victoria 3169, Australia*
[c] *National Institute of Standards and Technology, Gaithersburg, MD 20899, USA*
[d] *CNRS Laboratoire de Cristallographie, BP166, 38042 Grenoble, France*

Received 26 August 2002; accepted 19 November 2002

Abstract

The perovskite-related phase $Ca_3Nb_2O_8$, when grown as single crystals from a calcium vanadate flux, incorporates a small amount of vanadium from the flux to form the composition $Ca_3Nb_{2-x}V_xO_8$ with $x=0.05$. The crystals have pseudo-cubic symmetry with $a=6\times a_c$(perovskite). The actual symmetry is rhombohedral, space group $R3$, with $a_h=16.910(1)$ Å, $c_h=41.500(2)$ Å. The structure was solved using a combination of single-crystal methods together with constrained refinements of powder X-ray and neutron powder data. The unit-cell composition is $[Ca_{138}\square_{24}]_A\,[Ca_{42}Nb_{117}V_3]_B[O_{480}\square_6]$, with vacancies in both the anion sites and A-cation sites. The Ca and Nb atoms are fully ordered in the B-sites such that (001) layers containing only Nb-centered octahedra alternate with layers containing both Nb-centered and Ca-centered octahedra. At the origin B-site, ordered oxygen vacancies result in the octahedron being transformed to a tetrahedron, which, in the single crystals, is occupied by vanadium. The structure displays a new type of octahedral tilt system in which $3\times3\times3$ blocks of $(a^+a^+a^+)$ tilts are periodically twinned on the pseudo-cubic $\{1\,0\,0\}_c$ planes.

1. Introduction

A new perovskite-related phase with composition $3CaO{:}Nb_2O_5$ in the system $CaO–Nb_2O_5$ was reported by Ibrahim et al. [1]. They described two different crystallographic forms, I and II, for which the powder patterns were indexed in terms of a cubic cell with $a=23.934=6\times a_c$ (subscript c refers to the perovskite cubic subcell) and an orthorhombic cell, respectively. A subsequent phase equilibria study by Jongejan [2] reported that the shape of the liquidus curve was not consistent with the composition $Ca_3Nb_2O_8$. He proposed that the stable phase was not the 3:1 but the 4:1 composition $Ca_4Nb_2O_9$, consistent with the results of a study by Prince and Wilkins [3]. Hervieu et al. [4] confirmed the difficulty of synthesizing the 3:1 phase. Their preparations in air at 1400°C gave the $6\times a_c$ perovskite superstructure together with both $Ca_2Nb_2O_7$ and $Ca_4Nb_2O_9$ as impurity phases. These two phases also have perovskite-related structures [5,6] and compositionally lie to either side of the 3:1 phase.

Hervieu et al. [4] succeeded in preparing a single-phase product by heating the 3:1 molar mixture in argon at 1600°C. However, the phase had undergone partial reduction to a composition $Ca_3Nb_2O_{7.9}$. Electron diffraction patterns for this reduced phase were indexed with a tetragonal cell, $a_t=23.90/\sqrt{2}$ Å, $c_t=23.73$ Å. A complete structure determination was not undertaken, but the authors proposed that the structure contained Nb and Ca atoms distributed over the perovskite octahedral B-sites and that some of the A-sites were unoccupied. They also proposed that the B-site atoms were ordered such that alternate $(1\,1\,1)_c$ layers containing only niobium atoms alternated with layers containing a mixture of calcium and niobium atoms. Their model was described by the unit cell formulation $[Ca_{97}vac_{11}]_A[(Nb_{54})_B(Nb_{28}Ca_{26})_{B'}]O_{324}$.

A recent phase equilibria study [7] of the $CaO–Nb_2O_5$ system undertaken in air for the composition range 70–90 mol% CaO showed that reaction of the 3:1 molar composition gave a small amount of $Ca_2Nb_2O_7$ as impurity phase. A single-phase product was obtained at the molar composition 75.25% CaO + 24.75% Nb_2O_5. It decomposed above 1475°C to give $Ca_4Nb_2O_9$ (ss) and $Ca_2Nb_2O_7$. A powder XRD pattern for the pure phase

*Corresponding author. Fax: +61-3-9562-8919.
E-mail address: ian.grey@csiro.au (I.E. Grey).

0022-4596/03/$ - see front matter © 2003 Elsevier Science (USA). All rights reserved.
doi:10.1016/S0022-4596(03)00011-2

could be indexed using a cubic cell with $a = 23.93$ Å for $d > 1.3$ Å. However, higher angle reflections showed splitting consistent with a departure from cubic symmetry. Dielectric measurements showed that the ~3:1 phase has a dielectric constant of 50, which is ~50% higher than those for $Ca_4Nb_2O_9$ and $Ca_2Nb_2O_7$, and a temperature coefficient of permittivity of opposite sign to the latter two phases. The study also demonstrated that single crystals of $Ca_3Nb_2O_8$ could be prepared by flux growth, thus opening the possibility of a crystal structure analysis to help understand the reasons for the different dielectric behavior. We report here the results of a structure determination from single-crystal X-ray diffraction studies, supported by results from powder XRD and neutron diffraction refinements.

2. Experimental

2.1. Crystal growth and analyses

The composition $Ca_3Nb_2O_8$ was prepared first in sintered form, by solid-state reaction at 1375°C of a 3:1 molar ratio of CaO (99.999%) and Nb_2O_5 (99.998%). The sintered product was ground with an equal weight of vanadate flux of the same molar composition, $Ca_3V_2O_8$. The mixture was dried at 300°C then sealed in a 5 mm diameter platinum tube, which was suspended in a vertical quench furnace. The tube was heated to 1500°C at 300°C/h, held for 2 h, then cooled to 1300°C at 1°C/h and removed from the furnace. The pale yellow, euhedral crystals of $Ca_3Nb_2O_8$ were separated from the flux by washing in dilute HCl. They were characterized by wavelength dispersive electron microprobe analysis using a JEOL Superprobe operated at 15 keV. Standards used were wollastonite, $CaSiO_3$, niobium metal and vanadium metal.

2.2. Crystal data

Precession photographs confirmed a pseudocubic cell with a cell dimension six times the perovskite aristotype. The nature of the departure from cubic symmetry could not be resolved using the precession photos. There was no evidence of splitting of reflections that would occur if twinning by the pseudocubic symmetry elements were present. An optical microscopy examination showed that the crystals were weakly birefringent. A transmission electron microscopy examination [8] showed irregular submicron-scale domain boundaries, which displayed the characteristics of inversion twin domains.

For the intensity data collection a small (maximum dimension 0.1 mm) lath-shaped crystal was mounted on a Nonius Kappa diffractometer employing a CCD area detector and Mo$K\alpha$ radiation. An intensity data set was collected by rotating about ϕ, comprising 2×180 frames at 2° steps, with a counting time of 80 s per frame. The data set was fully indexed using a rhombohedral cell with $a_h = 16.90$ Å, $c_h = 41.50$ Å. This cell was in turn used to index a powder XRD pattern for the pure sintered phase (75.25 mol% CaO) which was then refined to obtain the cell parameters $a_h = 16.910(1)$ Å, $c_h = 41.500(2)$ Å. The CCD data were corrected for absorption and averaged using the different possible rhombohedral symmetries consistent with the systematic absences. The lowest R_{merg} was obtained for the Laue symmetry -3, for which merging of 46,630 reflections gave 10,902 unique reflections with $R_{merg} = 0.06$.

In view of the very small departure from cubic symmetry, some care was taken to check if the crystal was twinned on one of the pseudo-cubic symmetry elements. 3-D CCD scans were made on all equivalent reflections for a number of high-angle reflections ($d < 0.57$) using Ag$K\alpha$ radiation. An inspection of the images showed all reflections to be single peaks with no indication of adjacent twinned individuals.

2.3. Structure determination

2.3.1. Analysis of subcell reflections

Initially, the structure was assumed to be centrosymmetric (R-3). On this basis, the Patterson map was analyzed to determine the ordering of Ca and Nb atoms over the metal atom positions. Only a small number of oxygen atoms could be found in Fourier maps and the R factor remained high at 30%. The non-centrosymmetric space group $R3$ was then considered, allowing more oxygen atoms to be found and reducing the R factor to 19%. However, it was not possible to obtain a full set of oxygen atom positions from subsequent Fourier maps and a number of the O–O distances were unreasonably short. In view of the difficulty of establishing models for this type of highly pseudo-symmetric structure, in which the vast majority of reflections are weak superlattice reflections due to small deviations from the perovskite aristotype structure, it was decided to first work with only the subcell reflections (indexable by a 4 Å cubic perovskite cell). This type of approach can give useful information on the average cation site occupancies and on the mean directions and displacements of the atoms, particularly those of the anions due to octahedral tilting.

A total of 30 subcell reflections was used in $Pm3m$. Ca was placed in the A-site and Nb in the B-site. The oxygen atom was located in a difference Fourier synthesis. It was found not to reside at the expected ideal position $0, \frac{1}{2}, \frac{1}{2}$ but instead was distributed over the positions $0, x, x$ with $x \sim 0.42$. That is, the oxygen atoms were displaced along $\langle 110 \rangle_p$ directions by ~0.45 Å from the ideal perovskite anion site. Refinement of the cation site occupancies gave values less than 1 for both sites, which can be explained by vacancies at the A sites and substitution of Ca for Nb in the B sites

according to the model proposed by Hervieu et al. [4]. The refinement of the subcell reflections converged at an R value of 0.028.

2.3.2. Octahedral tilt model

Although the structure analysis, at this point, in space group $R3$ using the full CCD data set was unsuccessful in obtaining a complete model that could be refined, enough information was obtained on the oxygen atom positions to reveal a particular pattern of tilting of the octahedra. When the structure was viewed along each of the pseudo-cubic axes, it was apparent that three successive $\{1\,0\,0\}_c$ layers of octahedra were rotated in the same direction about the axis normal to the plane, followed by three layers that were rotated in the opposite direction. A model was constructed for this tilt system in $R3$, in which the angle of tilt was estimated from the oxygen displacements obtained in the analysis of subcell reflections. The tilt model agreed with the analysis of the subcell reflections in having all oxygen atom displacements directed along $\langle 110 \rangle_c$. The full symmetry of this ideal tilt model, with all tilt angles equal, was checked using the Addsym function within Platon [9] and was found to be R-3c. When referred to pseudocubic axes, it requires the full dimensions of the $6 \times a_c$ supercell (F-centered) for its description.

2.3.3. Structure refinement

Programs used for the single crystal refinement were SHELXL97 [10] and JANA [11]. The octahedral tilt model for the oxygen atoms was combined with the model for the metal atom ordering, but it was still not possible to refine the single-crystal data below an $R1$ (F) value of $\sim$20%. At this stage some form of micro-twinning was suspected and so it was decided to progress the refinement with powder data, for which both neutron diffraction and X-ray diffraction data had been collected. The program GSAS [12] using the EXPGUI interface (developed by B. Toby) was employed, which allowed the use of an extensive system of restraints on the Ca–O, Nb–O and O–O distances (total of 565 bond restraints). The chemical composition was also used as a constraint in the refinement to ensure that the correct number of A-site vacancies and B-site distribution of Ca and Nb was maintained. Alternating refinements were conducted on the XRD and ND data, with the XRD data used for the refinement of the metal atom positions and site occupancies, and the ND data used for the refinement of the oxygen atom positions. It was found necessary to weight the two data sets via the GSAS Histogram Weighting such that the XRD data had about one-third as much influence as the ND data. The refinements were initiated in the centro-symmetric space group R-3. It was found that significant improvements could be made to the fits by removing the center of symmetry and refining in $R3$. The refinements converged progressively to final values of $R(F^2) = 0.15$ for the ND data and $R(F^2) = 0.16$ for the XRD data. Although much lower $R(F^2)$ values ($\sim$0.04–0.07) could be obtained by relaxing the constraints, the refined models contained some unreasonable bond distances.

The refined model from the constrained powder refinements was then used as a starting model for refining the CCD data in the space group $R3$. This time the single-crystal refinement converged. This is believed to be due to the success of the constrained powder refinement in modifying the ideal oxygen tilt system to give the required large differences in bond lengths for the Ca-centered octahedra (Ca–O $\sim$ 2.3 Å) and the Nb-centred octahedra (Nb–O $\sim$ 1.95 Å). After removal of some atoms and relocation of others via difference Fourier maps, refinement with isotropic thermal parameters converged at $R = 0.08$. A plot of the structure showed that the major change relative to the powder refinement was that two of the oxygen atoms associated with the metal atom at the perovskite B-atom site at the origin were found to have zero occupancy and the remaining four oxygen atoms had undergone significant displacements to produce tetrahedral coordination. Furthermore, these oxygen sites were split into two sets of almost equal occupancy, defining tetrahedra pointing in opposite directions along the three-fold axis.

The tetrahedral bond distances were in the range 1.67–1.71 Å.These distances are too short to be Nb–O distances (ionic radius for 4-coordinated Nb^{5+} is 0.48 Å [13]). In addition, the refined site occupation factor with Nb at the origin was only 0.6. These two factors strongly indicated that the origin site was in fact occupied by vanadium, which was possible given that the crystals were grown from a vanadate flux. An electron microprobe analysis was conducted on the crystals, confirming the presence of vanadium. The analyses obtained were 40.6 wt% CaO, 58.4 wt% Nb_2O_5 and 1.5 wt% V_2O_5. The refinement further revealed that the eight A-atom sites surrounding the origin site were only partially occupied, by calcium. A constrained refinement of the occupancies of the two sets of oxygen atoms coordinating to the origin atom (constrained sum of occupancies of the two sets = 1), as well as a refinement of the occupancies of the surrounding A-sites was conducted, with vanadium at the origin. All coordinates and isotropic thermal parameters were refined, resulting in a factor $R1$ of 0.063 for $F > 4\sigma(F)$. Finally, all Ca and Nb sites were refined using SHELXL97 with anisotropic thermal parameters, resulting in convergence at $R1 = 0.047$ for 9058 reflections with $F > 4\sigma(F)$. For all 10,902 reflections, $R1 = 0.065$ and $wR2(F^2) = 0.11$.

Further refinements were conducted to check the possibility that the true symmetry was lower than rhombohedral and that apparent rhombohedral symmetry resulted from twinning about the pseudo-trigonal axis. The refinement was conducted using JANA, in the

triclinic space group $R1$ (the R-centered space group was used to maintain the spatial relationship to the rhombohedral cell). Twin domains corresponding to rotation about the pseudo-three-fold axis were generated in JANA. Refinement resulted in convergence at a similar R factor, but the refinement involved almost three times as many parameters as for the $R3$ refinement, and thus did not represent a real improvement on the $R3$ model.

The unit cell composition obtained from the structure refinement is $Ca_{180}Nb_{117}V_3O_{480}$. The calculated wt% values are 38.9% CaO, 60.0% Nb_2O_5 and 1.1% V_2O_5. The measured vanadia content is 1.5 wt%, suggesting that in addition to occupation of the tetrahedral site, there may be some substitution of V for Nb in the octahedral sites. Not surprisingly, at such a low level, this could not be verified from the structure refinement. If the V is grouped with the Nb then the formula is $Ca_{180}Nb_{120}O_{480} \equiv Ca_3Nb_2O_8$ (75 mol% CaO + 25 mol% Nb_2O_5). For convenience the composition $Ca_3Nb_2O_8$ will be used in the discussion section as shorthand for the actual V-containing composition for the flux-grown crystals.

A list of the coordinates, equivalent isotropic thermal parameters, number of atoms per site and site occupancies for the metal atoms from the final refinement in $R3$ is given in Table 1(a). Refined coordinates and isotropic thermal parameters are given in Table 1(b). A list of anisotropic thermal parameters can be obtained from the authors.

3. Results and discussion

$Ca_3Nb_2O_8$ has a superstructure of the perovskite structure due to ordering of Ca and Nb atoms on the B sites and ordering of Ca atoms and vacancies on the A sites. The B-site ordering is broadly as proposed by Hervieu et al. [4], in which (001) layers ($=(111)_c$) containing only Nb in the B sites alternate with layers containing both Nb and Ca. This alternation of B-site ordering is illustrated in Fig. 1, which is a projection of the structure along [110], showing Nb-centered octahedra in light shading and Ca-centered octahedra in dark shading (A-site cations not shown for clarity). Fig. 1 also illustrates the perturbation to the corner-connected octahedral framework at the origin where the B-site octahedron is replaced by a tetrahedron. The tetrahedral site is occupied by vanadium, with V–O distances consistent with the ionic radius for 4-coordinated V^{5+} [13]. The bond distances for the different B-site atoms are listed in Table 2. Except for the Ca(6) and Ca(7) polyhedra which are distorted through articulation with the VO_4 tetrahedra, the Ca–O distances are within a narrow range of 2.27–2.40 Å. The Nb–O distances cover a much wider range from 1.82 to 2.37 Å. Similar wide ranges are observed in the Nb_2O_5 polymorphs [14]. Average bond distances for each of the A-site Ca atoms together with the range of A-site distances are given in Table 3. Both the coordination number and the average bond distances are significantly lowered relative to an ideal perovskite structure (12 A–O at 2.82 Å for a 23.93/6 = 3.99 Å cell), due to the combined effects of octahedral tilting and B-site Ca/Nb ordering.

The B-site ordering model of Hervieu et al. [4] did not consider how the Nb and Ca atoms were ordered within the individual (001) layers. This intra-layer metal atom ordering is easily determined from Table 1(a), in which the B-site atoms in individual (001) layers (same $\pm z$ values) are grouped together and the number of atoms per site are given. Each layer contains nine B-site atoms. From Table 1(a) the occupation of six successive (001) layers, starting at $z = -0.17$ is: (2Ca + 7Nb), (9Nb), (6Ca + 3Nb), (8Nb + V), (6Ca + 3Nb), (9Nb). This sequence is repeated three times by the rhombohedral symmetry to give the total B-site contents per unit cell of $[Ca_{42}Nb_{117}V_3]$.

The ordering of Ca atoms and vacancies in the A sites can also be deduced from Table 1(a). The highest concentration of A-site vacancies occurs in the (001) layers on either side of the origin where the perovskite framework is modified by replacement of a B-site octahedon by a tetrahedron. These layers, at $z = \pm 0.03$, together with the equivalent layers generated by the $R3$ symmetry, contain 40.2Ca + 13.8 vacancies in the A-sites. The next pair of layers, at $z = \pm 0.08$ and their equivalents, contain a total of 43.8Ca + 10.2 vacancies in the A-sites. This includes two three-fold sites at $\pm(2/3,1/3,0.08)$, not listed in Table 1(a) because the refinement showed that these sites were completely vacant. The third pair of independent (001) layers of A-sites, at $z = \pm 0.14$ and their equivalents, have all A-sites occupied = 54Ca. The total A-site contents per unit cell is thus $[Ca_{138}\ \square_{24}]$, where $\square$ = vacancy. Combining the A- and B-site contents with the number of oxygen atoms per unit cell gives the full unit-cell composition: $[Ca_{138}\ \square_{24}]_A\ [Ca_{42}Nb_{117}V_3]_B[O_{480}\ \square_6]$. Relative to a stoichiometric perovskite composition $162[ABO_3]$, there are vacancies in both the A-atom sites and the anion sites. The anion vacancies are due to the change from octahedral to tetrahedral coordination of the B-site atom at the origin.

In Table 1(a), the metal atoms with coordinates of $\pm(x,y,z)$ are grouped in pairs to illustrate their close approximation to a centrosymmetric distribution. The B-site atoms are almost exactly related by an inversion center, with respect to both atom type (Ca or Nb) and position. Most of the A-site atoms are also centrosymmetrically related. The exceptions are the pairs of sites Ca(27), Ca(28) and Ca(35), Ca(36), which contain unequal occupations by Ca atoms. These A-sites are the first-nearest neighbor metal atom sites to the VO_4 tetrahedra. In Table 1(b), the oxygen coordinates with

Table 1
(a) *Metal atom coordinates* ($\times 10^4$) *and equivalent isotropic displacement parameters* ($A^2 \times 10^3$). $U(eq) = 1/3$ *of the trace of the orthogonalized* U_{ij} *tensor*

Atom	No.	Occupancy	*x*	*y*	*z*	*U*(eq)
B cations						
V(1)	3	1	0	0	−8(1)	10(1)
Nb(2)	9	1	3255(1)	−28(1)	23(1)	5(1)
Nb(3)	9	1	6737(1)	−3(1)	12(1)	7(1)
Nb(4)	3	1	3333	6667	28(1)	7(1)
Nb(5)	3	1	6667	3333	3(1)	3(1)
Ca(6)	9	1	894(1)	1845(2)	490(1)	13(1)
Ca(7)	9	1	9056(2)	8091(2)	9552(1)	15(1)
Ca(8)	9	1	4492(2)	2245(2)	590(1)	8(1)
Ca(9)	9	1	5405(2)	7716(2)	9468(1)	15(1)
Nb(10)	9	1	1142(1)	5592(1)	580(1)	4(1)
Nb(11)	9	1	8868(1)	4435(1)	9453(1)	4(1)
Nb(12)	9	1	2180(1)	1077(1)	1103(1)	4(1)
Nb(13)	9	1	7829(1)	8932(1)	8919(1)	7(1)
Nb(14)	9	1	5531(1)	1097(1)	1134(1)	5(1)
Nb(15)	9	1	4452(1)	8919(1)	8904(1)	5(1)
Nb(16)	9	1	2233(1)	4452(1)	1137(1)	5(1)
Nb(17)	9	1	7767(1)	5554(1)	8914(1)	5(1)
Ca(18)	3	1	0	0	1687(1)	8(1)
Ca(19)	3	1	0	0	8294(1)	10(1)
Nb(20)	9	1	3354(1)	−8(1)	1698(1)	2(1)
Nb(21)	9	1	6695(1)	59(1)	8354(1)	5(1)
Nb(22)	3	1	3333	6667	1704(1)	5(1)
A cations						
Ca(23)	9	1	2100(2)	4294(2)	326(1)	14(1)
Ca(24)	9	1	7764(2)	5582(2)	9749(1)	22(1)
Ca(25)	9	1	5545(2)	1090(2)	284(1)	12(1)
Ca(26)	9	1	4518(2)	9044(2)	9770(1)	11(1)
Ca(27)	0.8	0.087(6)	2621(20)	1357(20)	316(7)	10(1)
Ca(28)	3.4	0.374(7)	7347(3)	8703(3)	9676(1)	10(1)
Ca(29)	9	1	3308(2)	31(2)	859(1)	14(1)
Ca(30)	9	1	6659(2)	−25(2)	9200(1)	26(1)
Ca(31)	3	1	3333	6667	839(1)	6(1)
Ca(32)	3	1	6667	3333	9182(1)	12(1)
Ca(33)	9	1	6725(2)	28(2)	826(1)	13(1)
Ca(34)	9	1	3259(2)	−57(2)	9205(1)	10(1)
Ca(35)	0.0	0.015(9)	0	0	993(12)	10(1)
Ca(36)	1.8	0.609(12)	0	0	9015(2)	10(1)
Ca(37)	9	1	1181(2)	2237(2)	1387(1)	23(1)
Ca(38)	9	1	8898(2)	7720(2)	8690(1)	13(1)
Ca(39)	9	1	4316(2)	2194(2)	1439(1)	10(1)
Ca(40)	9	1	5568(2)	7818(2)	8620(1)	12(1)
Ca(41)	9	1	1063(2)	5506(2)	1376(1)	6(1)
Ca(42)	9	1	8960(2)	4474(2)	8611(1)	8(1)

(b) *Oxygen atom coordinates* ($\times 10^4$) *and isotropic displacement parameters* ($A^2 \times 10^3$)

Atom	*x*	*y*	*z*	*U*(eq)
O(1)	478(4)	2945(4)	379(1)	10(1)
O(2)	9205(4)	6912(4)	9754(2)	14(1)
O(3)	2139(4)	2860(4)	205(1)	13(1)
O(4)	7606(4)	7403(4)	9727(2)	20(1)
O(5)	370(4)	4580(4)	313(2)	15(1)
O(6)	9345(4)	5304(4)	9801(2)	13(1)
O(7)	2282(4)	5807(4)	389(1)	9(1)
O(8)	7726(3)	3582(3)	9674(1)	4(1)

Table 1 (*continued*)
(b) *Oxygen atom coordinates* ($\times 10^4$) *and isotropic displacement parameters* ($A^2 \times 10^3$)

Atom	*x*	*y*	*z*	*U*(eq)
O(9)	946(4)	6385(4)	312(2)	15(1)
O(10)	9546(4)	3893(4)	9624(1)	13(1)
O(11)	5592(4)	3100(4)	218(1)	11(1)
O(12)	4333(4)	7592(4)	9827(2)	19(1)
O(13)	3943(4)	3138(4)	361(1)	12(1)
O(14)	5850(4)	7079(4)	9866(2)	15(1)
O(15)	4114(4)	1182(4)	180(1)	11(1)
O(16)	6056(4)	9168(4)	9671(1)	14(1)
O(17)	1636(4)	−127(4)	963(2)	13(1)
O(18)	8020(4)	−63(4)	9171(2)	14(1)
O(19)	1897(4)	1684(4)	804(2)	16(1)
O(20)	8588(4)	8596(4)	9126(2)	15(1)
O(21)	2013(5)	3485(5)	881(2)	16(2)
O(22)	8005(5)	6601(5)	9151(2)	16(2)
O(23)	1406(4)	4726(4)	890(1)	11(1)
O(24)	8172(4)	5060(4)	9280(1)	9(1)
O(25)	1978(4)	6667(4)	896(2)	13(1)
O(26)	8335(4)	3512(4)	9081(2)	11(1)
O(27)	5210(4)	−195(4)	898(1)	6(1)
O(28)	5383(4)	183(4)	9141(1)	6(1)
O(29)	4846(4)	3274(4)	1004(2)	15(1)
O(30)	4960(4)	6295(4)	9265(1)	12(1)
O(31)	4988(4)	1285(4)	777(1)	13(1)
O(32)	5177(4)	8441(4)	9043(1)	12(1)
O(33)	3385(4)	1435(4)	963(2)	16(1)
O(34)	6653(4)	8070(4)	9109(2)	15(1)
O(35)	1373(4)	978(4)	1450(1)	12(1)
O(36)	8697(4)	9677(4)	8592(2)	15(1)
O(37)	2750(4)	598(4)	1522(2)	14(1)
O(38)	6955(4)	9232(4)	8598(2)	13(1)
O(39)	2982(4)	2552(4)	1335(2)	14(1)
O(40)	7511(4)	7740(4)	8600(2)	14(1)
O(41)	3048(4)	4272(4)	1450(2)	14(1)
O(42)	7324(4)	5952(4)	8543(1)	10(1)
O(43)	2513(4)	5589(4)	1438(2)	14(1)
O(44)	7488(4)	4374(4)	8658(2)	12(1)
O(45)	2470(4)	87874)	1442(2)	15(1)
O(46)	7147(4)	970(4)	8739(1)	9(1)
O(47)	5594(4)	2008(4)	1397(2)	16(1)
O(48)	3684(4)	8021(4)	8622(2)	15(1)
O(49)	4166(4)	231(4)	1328(1)	7(1)
O(50)	5438(4)	9553(4)	8523(1)	11(1)
O(51)	5853(4)	464(4)	1528(1)	9(1)
O(52)	3931(4)	9762(4)	8722(1)	6(1)
O(53)*	1067(10)	457(10)	145(4)	31(2)
O(54)*	427(12)	9329(12)	9863(4)	31(2)
O(55)*	0	0	9590(6)	31(2)
O(56)*	0	0	404(7)	31(2)

*Occupancies are 0.56(1) for O(53) and O(55), and 0.44(1) for O(54) and O(56).

approximate coordinates $\pm(x,y,z)$ are also grouped in pairs. In contrast to the metal atoms, there are large deviations from centrosymmetric relationships for the coordinates of many of the oxygen atom pairs.

The non-centrosymmetrical character of the $Ca_3Nb_2O_8$ structure is primarily related to the directional character of the VO_4 tetrahedron at the origin. The refinement showed that the oxygen distribution around the origin corresponds to two opposing orientations of the tetrahedra (with the apex oriented in $+z$ and $-z$ directions) occurring with approximately equal probabilities. This is consistent with the observation of inversion twin micro-domains by transmission electron microscopy [8], in which the tetrahedra will be all oriented in one or other of the two possible orientations with respect to the trigonal axis. As mentioned above, the A-sites closest to the origin also contribute significantly to the non-centrosymmetrical character by

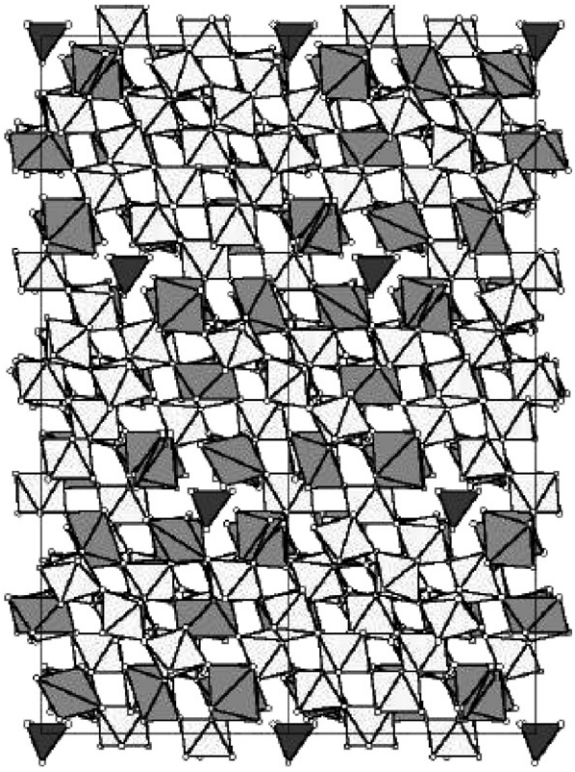

Fig. 1. [110] projection of the B-site octahedral framework in $Ca_3Nb_2O_8$. Nb-centered and Ca-centered octahedra have light-gray and medium-gray shading, respectively. The B-site at the origin contains tetrahedrally coordinated vanadium (dark-gray). The unit-cell outline is shown; the [001] direction is vertical.

their unequal Ca occupancies. On the basis of the approximately equal amounts of the two VO_4 orientations, it might have been expected that the A-site Ca atoms surrounding the origin tetrahedra would form two subgroups, also with approximately equal occupations. In fact, the refinement showed quite variable occupation of the four surrounding A-site atoms, Ca(27), Ca(28), Ca(35) and Ca(36), ranging from 1% to 60% occupation, see Table 1(a). The average occupation of the four A-sites is only 25%.

The relationship of the VO_4 tetrahedron to the surrounding B-site polyhedra and A-site atoms is illustrated in Fig. 2 for one of the orientations of the tetrahedron, $VO(56)O(54)_3$. The three B-site atoms Ca(7) have distorted octahedral coordination and maintain the topology of the perovskite structure by corner sharing to the triangular base of the VO_4 tetrahedron. The three other B-site atoms surrounding the origin site are seven-coordinated (mono-capped trigonal prismatic with O(21) the cap) and each one shares an edge with the VO_4 tetrahedron. Similar structural environments pertain for the other orientation of the tetrahedron, $VO(55)O(53)_3$. It is interesting to note that the six B-sites surrounding the VO_4 are all occupied by Ca, as are the surrounding A-sites, producing a local cluster enriched in calcium.

Apart from the perturbation due to the replacement of a B-site octahedron by a tetrahedron at the origin, the structure of $Ca_3Nb_2O_8$ is of the perovskite type and is closely approximated by the symmetry of the pseudo-cubic face-centered 6 x a_c cell. This is illustrated in Fig. 3 which shows three successive $(100)_c$ layers of B-atom centered polyhedra, viewed along the pseudo-cubic a_c axis. The same layer sequences are observed along each of the three pseudo-cubic axes. Two of the layers have the same composition and comprise the perovskite topology of corner-linked Ca- and Nb-centred octahedra. The Ca-centered octahedra form intersecting chains directed along $[011]_c$ and $[01-1]_c$ directions. The network of Ca-centered octahedral chains encloses square arrays containing 13 Nb-centered octahedra. The third layer contains the VO_4 tetrahedra, with the associated local modifications to the coordination of the nearest-neighbor B atoms. This layer contains predominantly Nb-centered octahedra with the Ca confined to clusters of four B-sites surrounding the VO_4 tetrahedra.

The corner-linked octahedral nets in each of the layers shown in Fig. 3 are seen to have undergone relatively large rotations ($\sim 11^\circ$) about the $[100]_c$ projection axis, deforming the square channels between the octahedra into rhombi. The orientations of the rhombi are consistent with the sign of the rotation being the same in each of the three layers. The next three $(100)_c$ layers following those shown in Fig. 3 have the octahedra rotated in the opposite direction. The same alternation of three clockwise rotations followed by three anti-clockwise rotations occurs about the other two pseudo-cubic axes, $[010]_c$ and $[001]_c$, as evidenced by the directions of the displacements of the apices of the octahedra in Fig. 3. In the diagram, the planar $(010)_c$ and $(001)_c$ boundaries across which the change of sign of the rotation occurs are marked by dashed lines.

Using the notation of Glazer [15], for which rotation in the same direction of adjacent layers of octaheda is specified as a^+ and rotation of adjacent layers in opposite directions is specified as a^-, the rotations along each pseudo-cubic axis for $Ca_3Nb_2O_8$ can be written as $a^+a^+a^-\ a^+a^+a^-$. The complete tilt system can be described as an $(a^+a^+a^+)$ tilt system which is periodically twinned on $\{100\}_c$ planes to produce elements of $(a^-a^-a^-)$ tilting. The pure $(a^+a^+a^+)$ tilt system has cubic symmetry, $Im3$ [15], and is well known in the families of compounds with general formula $ACu_3M_4O_{12}$ and $AMn_3M_4O_{12}$ [16], whereas the tilt system $(a^-a^-a^-)$ has rhombohedral symmetry, R-3c [15]. In $Ca_3Nb_2O_8$ the $(a^+a^+a^+)$ tilts occur in $3 \times 3 \times 3$ blocks bounded by $\{100\}_c$ planes, as shown in intersection in Fig. 3. Adjacent blocks have opposite signs of the rotation about the axis normal to the plane separating the blocks. It is interesting to note that Subramanian and Sleight [16] have recently proposed fine-scale multiple twinning across $\{100\}_c$ planar boundaries of

Table 2
Polyhedral bond lengths (Å) for B-sites

V(1)–O(53) (× 3)	1.69 (1)	Ca(9)–O(30)	2.290 (7)	Nb(15)–O(48)	1.843 (6)
–O(55)	1.67 (2)	–O(32)	2.290 (6)	–O(30)	1.866 (6)
V(1)–O(54) (× 3)	1.71 (2)	–O(12)	2.273 (7)	–O(32)	1.865 (6)
–O(56)	1.71 (2)	–O(16)	2.291 (7)	–O(52)	2.154 (5)
		–O(14)	2.293 (7)	–O(50)	2.156 (6)
Nb(2)–O(4)	1.829 (7)	–O(34)	2.401 (7)	–O(28)	2.156 (6)
–O(1)	1.877 (6)				
–O(14)	1.931 (6)	Nb(10)–O(5)	1.904 (6)	Nb(16)–O(21)	1.825 (7)
–O(15)	1.936 (6)	–O(9)	1.893 (6)	–O(25)	1.968 (6)
–O(10)	2.305 (6)	–O(7)	1.943 (5)	–O(23)	1.967 (6)
–O(5)	2.308 (6)	–O(27)	1.975 (5)	–O(45)	2.007 (6)
		–O(25)	2.110 (6)	–O(41)	2.026 (6)
Nb(3)–O(3)	1.846 (6)	–O(23)	2.159 (6)	–O(43)	2.138 (6)
–O(2)	1.856 (6)				
–O(16)	1.918 (6)	Nb(11)–O(10)	1.928 (6)	Nb(17)–O(22)	1.886 (7)
–O(13)	1.928 (6)	–O(28)	1.961 (5)	–O(42)	1.971 (6)
–O(6)	2.281 (6)	–O(6)	1.928 (6)	–O(26)	2.004 (6)
–O(9)	2.327 (6)	–O(8)	1.967 (5)	–O(46)	1.986 (6)
		–O(26)	2.054 (6)	–O(24)	2.013 (6)
Nb(4)–O(12) (× 3)	1.834 (6)	–O(24)	2.063 (6)	–O(44)	2.094 (7)
–O(7) (× 3)	2.221 (6)				
		Nb(12)–O(19)	1.819 (6)	Ca(18)–O(35) (× 3)	2.293 (6)
Nb(5)–O(11) (× 3)	1.880 (6)	–O(17)	1.859 (6)	–O(48) (× 3)	2.341 (6)
–O(8) (× 3)	2.121 (5)	–O(33)	1.904 (6)		
		–O(35)	1.933 (6)	Ca(19)–O(47) (× 3)	2.274 (6)
*Ca(6)–O(19)	2.261 (6)	–O(37)	2.323 (6)	–O(36) (× 3)	2.341 (7)
–O(3)	2.275 (6)	–O(39)	2.369 (6)		
–O(17)	2.318 (6)				
–O(1)	2.341 (6)	Nb(13)–O(20)	1.854 (6)	Nb(20)–O(40)	1.922 (6)
–O(56)	2.728 (4)	–O(18)	1.881 (6)	–O(37)	1.918 (6)
–O(54)	2.834 (18)	–O(36)	1.933 (6)	–O(49)	1.962 (5)
–O(21)	2.943 (7)	–O(34)	1.951 (6)	–O(52)	1.962 (5)
		–O(38)	2.229 (6)	–O(45)	2.114 (6)
*Ca(7)–O(4)	2.244 (7)	–O(40)	2.241 (6)	–O(42)	2.103 (6)
–O(20)	2.274 (7)				
–O(2)	2.291 (6)	Nb(14)–O(47)	1.847 (6)	Nb(21)–O(39)	1.913 (6)
–O(18)	2.331 (7)	–O(31)	1.852 (6)	–O(38)	1.946 (6)
–O(54)	2.571 (18)	–O(29)	1.843 (6)	–O(51)	1.960 (6)
–O(54)	2.941 (18)	–O(51)	2.169 (6)	–O(50)	1.981 (6)
–O(22)	2.795 (7)	–O(49)	2.178 (5)	–O(41)	2.063 (6)
		–O(27)	2.200 (5)	–O(46)	2.082 (6)
Ca(8)–O(33)	2.283 (7)				
–O(15)	2.321 (6)			Nb(22)–O(43) (× 3)	1.984 (6)
–O(11)	2.291 (6)			–O(44) (× 3)	2.003 (6)
–O(13)	2.336 (6)				
–O(31)	2.301 (6)				
–O(29)	2.302 (7)				

*Coordination of Ca(6) and Ca(7) shown for one tetrahedral orientation, $VO(56)O(54)_3$.

the $(a^+a^+a^+)$ tilt system in the cubic compound $CaCu_3Ti_4O_{12}$ as a possible extrinsic contribution to its very high dielectric constant.

Subramanian and Sleight mentioned the possibility of having compositional changes at the twin boundaries in the $ACu_3Ti_4O_{12}$ compounds [16]. Fig. 3 shows that for $Ca_3Nb_2O_8$ a compositional modification occurs adjacent to the intersection of the planar tilt boundaries, due to the replacement of an MO_6 octahedron by a MO_4 tetrahedron. In the flux grown crystals the tetrahedron is occupied by vanadium. However, samples prepared by solid-state reaction contain no vanadium yet still exhibit the same $6 \times a_c$ pseudo-cubic superstructure. It is not unreasonable that niobium occupies the tetrahedral site in this case. Tetrahedral coordination of niobium has been reported in H–Nb_2O_5 [14]. The structure of H–Nb_2O_5 is made up of blocks of perovskite-type corner-linked octahedra and the tetrahedra occur at the boundaries separating the blocks. The actual composition reported for single-phase calcium niobate is slightly removed from the 3:1 molar ratio to a more calcium-rich composition with 75.25 mol% CaO(7). If the same

Table 3
Average bond lengths and ranges of bond lengths for A-site atoms

Site	No. of bonds ($\leqslant 3$ Å)	Average	Range
Ca(23)	9	2.643	2.347–3.053
Ca(24)	8	2.611	2.337–2.946
Ca(25)	6	2.415	2.344–2.538
Ca(26)	8	2.546	2.327–2.734
Ca(27)	8	2.755	2.392–2.993
Ca(28)	8	2.642	2.413–2.971
Ca(29)	8	2.607	2.343–3.054
Ca(30)	8	2.600	2.311–2.978
Ca(31)	9	2.591	2.304–2.982
Ca(32)	12	2.702	2.608–2.782
Ca(33)	8	2.590	2.281–3.104
Ca(34)	7	2.516	2.310–2.957
Ca(35)	8	2.800	2.448–2.884
Ca(36)	8	2.576	2.389–2.991
Ca(37)	9	2.660	2.325–3.058
Ca(38)	9	2.628	2.347–3.047
Ca(39)	8	2.554	2.343–2.724
Ca(40)	6	2.418	2.308–2.624
Ca(41)	8	2.487	2.343–2.680
Ca(42)	10	2.601	2.417–2.871

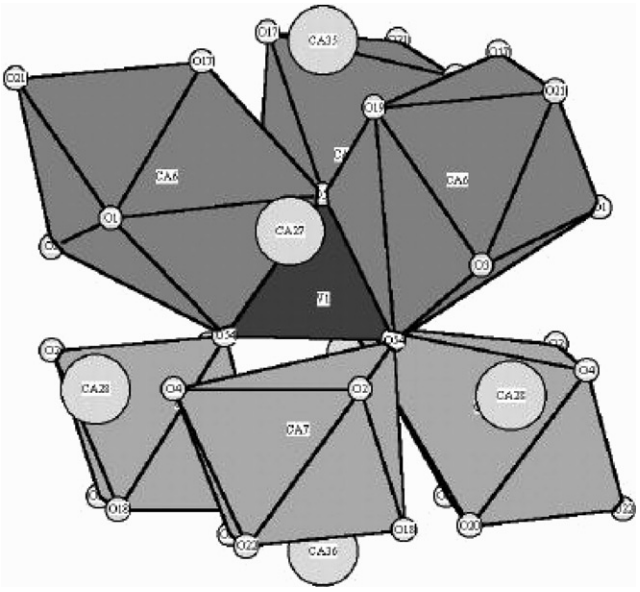

Fig. 2. Structure around the VO_4 tetrahedron at the origin.

structure is maintained as for the flux-grown crystals, with three tetrahedra per unit cell, then the observed composition requires a slightly higher occupation of both the A-sites and the B-sites by calcium. In recent unpublished work at NIST it has been found that single-phases can be prepared at compositions up to 75.5 mol% CaO. The rhombohedral distortion from a metrically cubic cell decreases with increasing CaO content. Further studies are warranted to determine the effects of these subtle compositional changes on the dielectric properties.

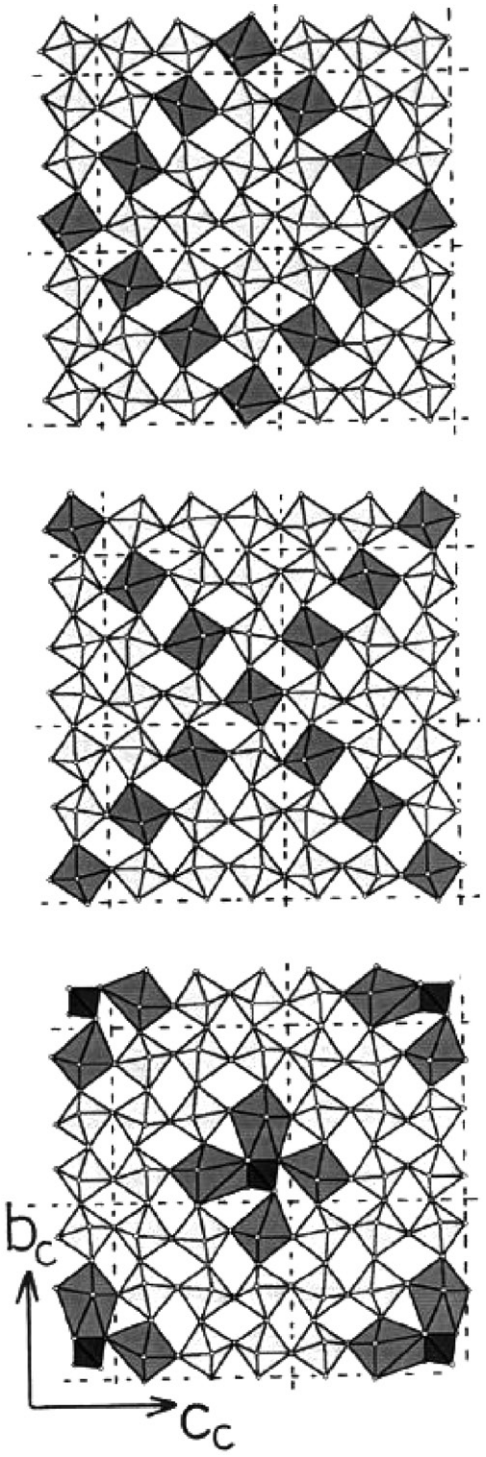

Fig. 3. Three successive pseudo-cubic $(1\,0\,0)_c$ layers in $Ca_3Nb_2O_8$. Polyhedral shading as in Fig. 1. The dashed lines delineate the blocks of $(a^+a^+a^+)$ octahedral tilting.

Acknowledgments

We thank Julia Chan for preparation of the powder samples, Gary Fallon for the collection of the single crystal data, Qing Huang for the collection of powder

ND data, Nick Wilson for help with the electron microprobe analyses and Igor Levin for the transmission electron microscope observations. Thanks are due to Bob von Dreele and Brian Toby for modifications to GSAS and EXPUI, respectively, to improve the procedures for restrained refinement and weighting of different data sets, and to Tom Speck for modifications to the PLATON software.

References

[1] M. Ibrahim, N.F. Bright, J.F. Rowland, J. Am. Ceram. Soc. 45 (1962) 329.
[2] A. Jongejan, J. Less Common Metals 19 (1969) 193.
[3] A.T. Prince, A.L. Wilkins, Min. Sci. Div. Rept. MS64-63, Mines Branch, Department of Energy, Mines and Resources, Ottawa, 1964.
[4] M. Hervieu, F. Studer, B. Raveau, J. Solid State Chem. 22 (1977) 273.
[5] N. Ishizawa, F. Marumo, S. Iwai, M. Kimura, T. Kawamura, Acta Crystallogr. Sect. B 36 (1980) 763.
[6] I. Levin, L.A. Bendersky, J.P. Cline, R.S. Roth, T.A. Vanderah, J. Solid State Chem. 150 (2000) 43.
[7] T.A. Vanderah, W. Febo, J.Y. Chang, R.S. Roth, J.M. Loezos, L.D. Rotter, R.G. Geyer, D.B. Minor, J. Solid State Chem. 155 (2000) 78.
[8] I. Levin private communication, 2002.
[9] A.L. Speck, PLATON, a multipurpose crystallographic tool, Utrecht University, Utrecht, The Netherlands, 2001, http://www.cryst.chem.uu.nl/platon/.
[10] G.M. Sheldrick, SHELXL97, University of Gottingen, Germany, 1997.
[11] V. Petricek, M. Dusek, The Crystallographic Computing System JANA2000, Institute of Physics, Praha, Czech Republic, 2000.
[12] A.C. Larson, R.B. Von Dreele, General Structure Analysis System (GSAS), Los Alamos National Laboratory Report LAUR86-748, 1994.
[13] R.D. Shannon, Acta Crystallogr. Sect. A 32 (1976) 751.
[14] B.M. Gatehouse, A.D. Wadsley, Acta Crystallogr. 17 (1964) 1545.
[15] A.M. Glazer, Acta Crystallogr. Sect. B 28 (1972) 3384.
[16] M.A. Subramanian, A.W. Sleight, Solid State Sci. 4 (2002) 347.